C. R. Physique 3 (2002) 1423–1444

Physique appliquée/*Applied physics*

DOSSIER

MÉCANISMES PHYSIQUES DU NUAGE D'ORAGE ET DE L'ÉCLAIR
THE PHYSICS OF THUNDERCLOUD AND LIGHTNING DISCHARGE

The interaction between a lightning flash and an aircraft in flight

Anders Larsson

FOI – Swedish Defence Research Agency, Grindsjön Research Centre, 14725 Tumba, Sweden

Note presented by Guy Laval.

Abstract Roughly speaking, every commercial airliner is struck by lightning once per year. Thus, the lightning strike to aircraft is not uncommon and it poses an appreciable threat to flight safety. The understanding of the lightning strike to aircraft has been greatly enhanced during the last years thanks to a comprehensive analysis of data collected from instrumented aircraft that have been flown into thunderstorm regions. In this article, we will start with the phenomenology of the lightning strike to aircraft and continue with going deeper into the underlying physics of selected processes during the strike. ***To cite this article: A. Larsson, C. R. Physique 3 (2002) 1423–1444.***

lightning discharge / aircraft / leader / arc

Interaction d'un éclair et d'un avion en vol

Résumé En moyenne, chaque avion de ligne est foudroyé une fois par an. Le foudroiement d'un appareil n'est donc pas exceptionnel et constitue une menace non négligeable pour la sécurité des vols. La compréhension du processus de foudroiement a considérablement progressé ces dernières années, grâce à l'analyse exhaustive des données enregistrées à bord d'avions instrumentés volant dans des zones orageuses. Dans cet article, nous nous appuyons sur la description phénoménologique du foudroiement d'un appareil pour approfondir les bases physiques des différentes phases de l'éclair sur avion. ***Pour citer cet article : A. Larsson, C. R. Physique 3 (2002) 1423–1444.***

éclair / avion / leader / arc

1. Introduction

A lightning flash is a natural electrical discharge and direct lightning strikes to aircraft are events that must be considered in the design of aircrafts. In-flight statistics show that a commercial airliner can expect one lightning strike for somewhere between each 1000 and 10 000 hours of flight, where a generally accepted figure seems to be each 3000 hours of flight [1,2]. In general terms, this is equivalent to one lighting strike for each airplane each year. Thus, the lightning strike to an aircraft is not uncommon and

E-mail address: Anders.Larsson@foi.se (A. Larsson).

S1631-0705(02)01410-X/REV

it poses a potential threat to flight safety that must be recognised. Understanding the physical processes involved in lightning strikes to aircraft is essential for mainly two reasons: first, to correctly evaluate the electromagnetic threat to aircraft systems and second, for defining and developing test and design criteria of aircrafts and aircraft systems to certify them against lightning hazards. These issues are becoming more and more important since aircraft safety is increasingly more dependent on electronic equipment and the development of new materials. This increased dependency is caused by the fact that higher demands on safety in traffic control, environmental friendliness and fuel economy on air transport have often been met by more advanced technology (that is, by more electronics on aircraft and by the introduction of new materials into the aeronautics industry). Simultaneously, the replacement of metallic airframes by carbon composite materials with low electrical and thermal conductivities has reduced the electromagnetic shielding effectiveness of the construction materials and made them less resistive against the direct effects of a lightning strike. The lightning hazards to aircraft can be minimised in two ways. First, decrease the probability of lightning strikes to aircraft by avoiding thunderstorms regions, and, second, by hardening the aircraft and aircraft systems against the effects of a direct strike. The first option may reduce, but not eliminate, incidences, since take-offs and landings are generally well determined both in time and location. Thus, the aircraft and its systems must be hardened, and the physical processes during the strike must be understood to correctly evaluate the treat. This article is concentrated upon how the lightning channel interacts with the body of the aircraft, not the interference of the electromagnetic pulse with the aircraft and its system. The latter is a great topic in itself [3].

Our scientific knowledge of the physical processes that occur during a direct lighting strike to aircraft is based mainly upon three major research programmes studying the interaction between lightning and aircraft [4]:

(i) NASA Storm Hazards programme: F-106 aircraft, USA (1978–1986) [5];
(ii) USAF/FAA Lightning Characterisation programme: CV-580 aircraft, USA (1984–1985, 1987) [6];
(iii) ONERA/CEV Transall programme: C-160 aircraft, France (1984, 1988) [7].

These campaigns involved in-flight measurements with instrumented aircraft flying into thundercloud regions with the purpose of being struck by lightning. The interpretation of these in-flight data has greatly enhanced our understanding of the processes and the mechanisms. A comprehensive analysis of these data are summarised by Lalande et al. [8,9]. The in-flight measurements have shown that there are two different cases of a lightning strike to aircraft (Fig. 1). The first is the interception by the aircraft of a branch of a natural lightning leader developing in the vicinity of the aircraft. The second case is that the aircraft itself triggers the lightning discharge when it flies into a region of intense electric field or a highly charged region. That the aircraft itself can trigger a lightning discharge [10] was experimentally shown by Mazur et al. [11] using UHF band radar echoes of aircraft during thunderstorm penetrations. All lightning strikes to aircraft at high altitudes (>7 km) are of the second kind [11], that is, the aircraft triggered the lightning discharge. At low altitudes (<7 km), 90% of the strikes are aircraft-triggered [7].

A common feature of both these cases is that the lightning strike to aircraft starts with the development of a positive discharge from the aircraft, followed by, a few milliseconds later, the inception of a negative discharge propagating in the opposite direction (a bi-directional leader [10,12,13], as illustrated in Fig. 1. During the lightning flash, the aircraft forms a part of the lightning current path. Thus, there are two attachment points on the aircraft for the lightning current: one entry point and one exit point. The entry and exit points are defined as to the direction of the current. Thus, the exit point of the current will be at an anodic surface (positive electrode) and the entry point at a cathodic surface (negative electrode). As a result, the exit point is the attachment point of the positive leader and the entry point is the attachment point of the negative leader. The lightning current consists of a continuing current of about 300 A with a duration of about 200 ms, with superimposed high-amplitude currents (recoil leaders [14]). The data for the current impulses from the in-flight campaigns are uncertain because of poor sampling rate and other measurement problems. However, the measured peak current was up to 20 kA and its time derivative up to 10^{10} A·s^{-1} $=$ 10 kA·μs^{-1}. Furthermore, when the continuing current eventually has vanished, current

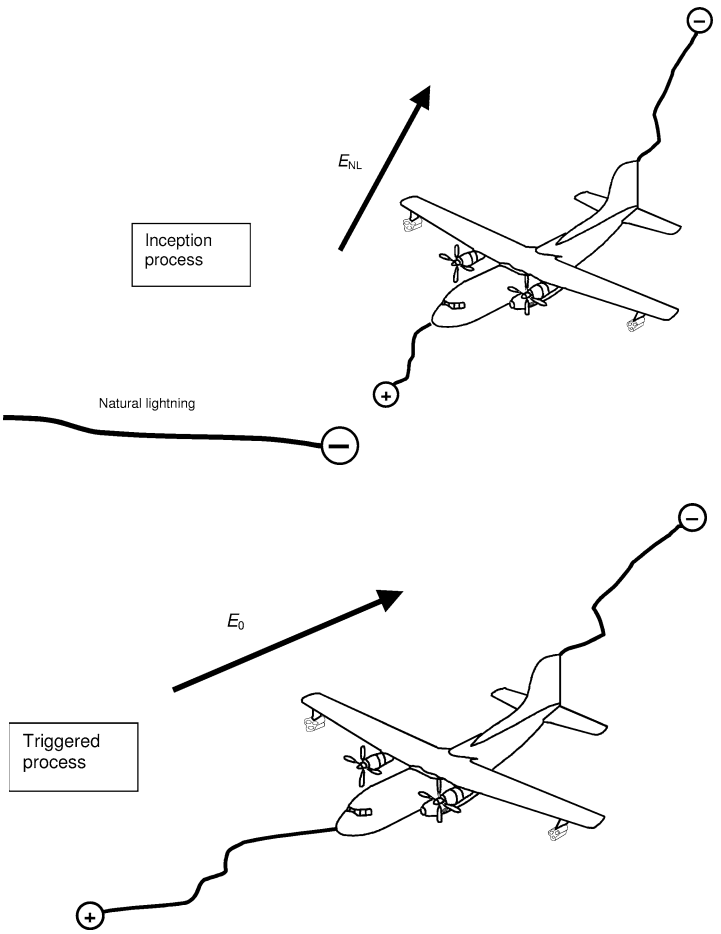

Figure 1. The two different processes that lead to a lighting strike to an aircraft through a bi-leader process. Above: the interception by the aircraft of a natural lightning discharge. Below: the aircraft itself triggers the lightning discharge. The aircraft-triggered process is the more common one.

impulses still may occur. For a typical waveform of the lightning current, see Fig. 2. The aircraft is a part of the current path of an intra-cloud or an inter-cloud lightning flash if the discharge is bi-directional during the whole flash. If one of the bi-directional leaders reaches the ground, the aircraft forms a part of a cloud-to-ground lightning flash. The latter is the case in 25% for low-altitude strikes (<7 km) [4].

The lightning channel is essentially stationary in the air while the aircraft is moving. Since the total duration of the lightning flash can be up to one second and considering typical aircraft speeds, the lightning channel can be displaced along the whole length of the aircraft during the flash – a so-called *lightning swept stroke*. The determination of the different areas or zones where the lightning channel may have its initial attachment point and where it might further attach or sweep over is called *aircraft zoning*. This article reflects our physical understanding of the lightning swept stroke and introduces a roadmap of how to implement this knowledge into an aircraft zoning design tool [15–18] and forms a part of the general increase of the understanding of the electromagnetic threat to aircraft [3].

A phenomenological description of the swept stroke follows. When the aircraft moves, the movement of the lightning channel along the aircraft depends upon the surface properties, the aerodynamic flow profile

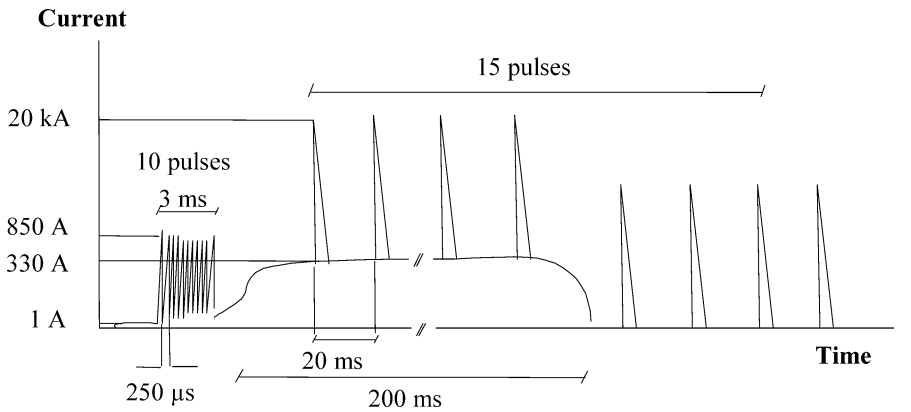

Figure 2. Typical waveform of the discharge current during a lightning strike to an aircraft as inferred from in-flight measurements [9].

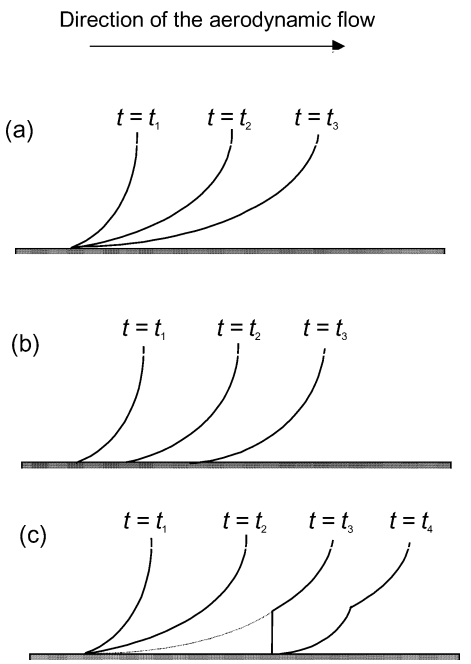

Figure 3. Illustrations of three different swept-stroke phenomena. The lines represent the position of the lightning channel. (a) The attachment point dwells at the same spot; (b) the attachment point sweeps continuously along the surface; and (c) a breakdown occurs between the channel and the surface (at $t = t_3$) and the attachment point makes a jump (a reattachment). The broken curve shows the short-circuited part of the channel.

and the plasma properties of the channel. Mainly two phenomena may occur at the attachment point of the lightning channel at the surface. Firstly, the attachment point may dwell at the same spot and thus follow the aircraft as it moves through the air (Fig. 3(a)). This results in a large deformation of the lightning channel. Secondly, the attachment point may continuously sweep along the surface (Fig. 3(b)). Another important phenomenon is the possibility of having a reattachment (or re-connection) between a segment of the channel and the surface (Fig. 3(c)). The voltage distribution along the channel is dependent on the lightning current and the plasma properties of the channel. This voltage distribution gives rise to the possibility of a dielectric breakdown of the air gap between the surface and a segment of the channel. During such a breakdown, the channel attachment point makes a jump. Reattachment can occur if the channel is substantially deformed or if the channel sweeps along a complex object where reattachment may occur to protruding parts.

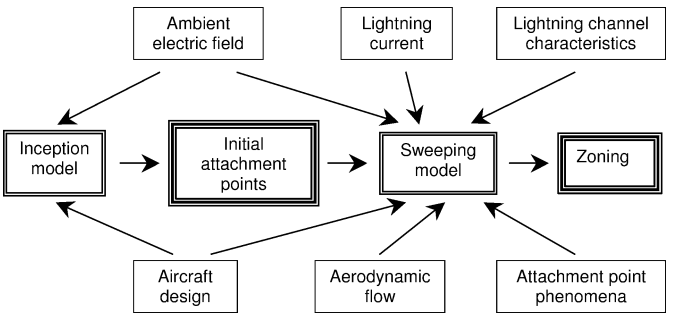

Figure 4. A roadmap towards a design tool to determine the initial attachment points and the swept stroke zones. The core of the roadmap is the two models of the lightning inception and lightning sweeping and their dependencies.

2. The zoning of aircraft

In the design of aircraft it is important do determine the locations of where the lightning can have its initial attachment points on the aircraft and over which areas the attachment point may sweep. The determination of these locations and areas are called *aircraft zoning* and a generic way of performing this zoning is shown in Fig. 4, where a roadmap towards a simulation tool to determine the lightning swept stroke zones is sketched. As shown in the figure, two physical processes must be modelled: the inception of the lightning flash and the sweeping of the lightning channel along the aircraft.

The points from where a stable-propagating lightning leader discharge can be initiated determine the locations of the initial attachment points. The initial attachment of a lightning channel occurs within a few milliseconds and is thus so rapid process that the sweeping phenomena can be neglected. The parameters that govern the location of the initial attachment points are the aircraft geometry and the ambient electric field.

The sweeping phase is more complex than the initial attachment phase, mainly because its longer duration (up to one second) which implies that considering typical aircraft speeds the lightning channel can be displaced along the whole aircraft during the existence of the lightning flash. As for the initial attachment, the aircraft design and the electric field environment are important factors, but also the interaction between the lightning current, the lightning channel characteristics and the aerodynamic flow must be considered.

A solution of the problem to determine the initial attachment points is concisely presented in the next section. The rest of the article is devoted to the lightning swept stroke.

3. Initial attachment points

As mentioned in the introduction, the initial attachment points at the aircraft are associated to positive and negative lightning leaders that are initiated at the aircraft itself (a bi-directional leader). This bi-directional leader is incepted in two phases [19]. The first phase is the inception of a positive leader propagating from the aircraft; an inception that is dependent on the ambient electrostatic field and the aircraft geometry. The second phase is the inception of the negative leader a few milliseconds later. The negative leader occurs after the positive one since the former has a higher threshold electric field for inception. The electric field environment for the inception of the negative leader is more complex than for the positive one since the presence of the positive leader alters the field distribution and since the current of the positive leader charges the aircraft.

To form an initial lightning attachment point at the aircraft, three conditions must be fulfilled [19], see Fig. 5. First, the ambient electric field must reach the corona inception field strength. Second, the corona current must heat the corona stem so a leader channel segment is created. Third, the dynamic coupling between the thermodynamic processes and the electric field distortion by the leader channel must favour

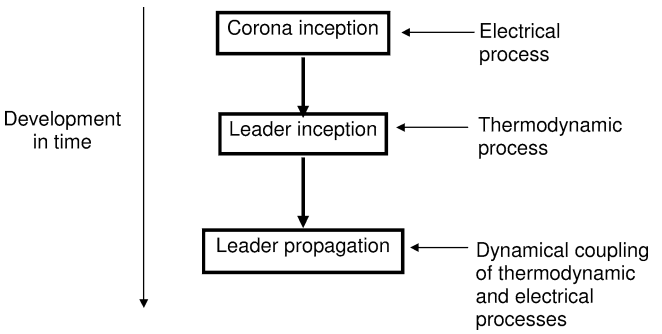

Figure 5. The three different conditions that must be fulfilled to form an initial attachment point of the lightning discharge at the aircraft. Adapted from Lalande et al. [19].

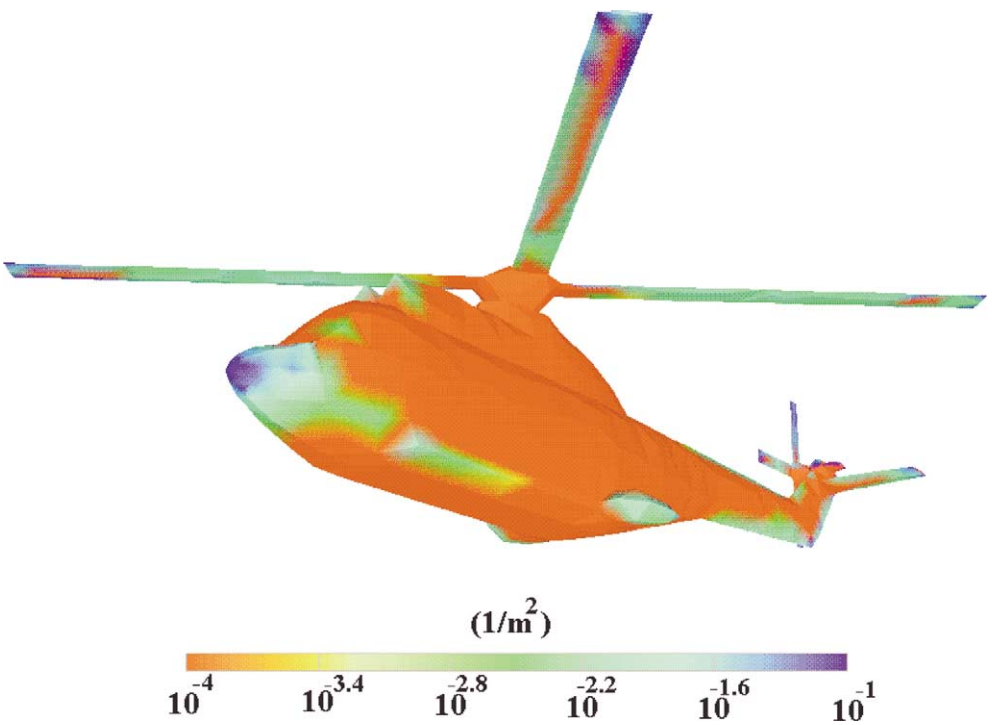

Figure 6. Calculation of probability density distribution for initial attachment points for an AS332 (Super Puma) helicopter.

a stable propagation of the discharge. Physical models of these three conditions has been successfully implemented into a simulation tool for determine the initial attachment points. An example of such a simulation is shown in Fig. 6 where the probability density distribution of initial attachment points is shown for a Super Puma helicopter. This probability density is calculated in the following way. For a given direction of the ambient electric field, the areas where initial attachment point can be present are calculated. Such a calculation is then repeated for all directions of the ambient field. Finally, the areas from all directions are integrated and expressed as a probability density distribution. See Lalande et al. [19] for details.

4. Aircraft design and aerodynamic flow

As obvious input data to any determination of swept stroke zones is the aircraft geometry, where the surface material and structure are of great importance. The different behaviour of bare metal surfaces and painted metal surfaces are discussed in Sections 7 and 8 below, which also have bearings on composite materials. Any complete zoning tool must have compliance with stealth technology. Of course, other airborne vehicles such as space shuttles must likewise be subjected to lightning strike zoning and the tools given in this article can be directly applied here too. With a general model for the zoning, also airborne vehicles with moving parts such as helicopters can straight forward be treated. Furthermore, the moving geometry of a helicopter has striking similarities with windmills. Thus, the lightning protection of windmills can in addition be supported by the information provided here [20].

To solve the general problem for the aerodynamic flow distribution around such a complex object as an aircraft in flight, the full non-linear Navier-Stokes equation must be solved including effects such as boundary layers, wakes, turbulence, supersonic flow, etc. [21]. Even if the problem is well defined, the complete problem is too complex and requires a too fine mesh and a too short time step to be numerically solvable with today's computers. However, within the scope of this article, the aerodynamic flow will be treated as an input data for the swept stroke calculations. The used approximations of the airflow are discussed in connection of the examples of swept stroke simulations presented in Section 10.

5. The voltage gradient along the lightning channel

One property of the lightning channel that is of central importance is its internal electric field strength or voltage gradient. This voltage gradient is the cause of the voltage build-up along the lightning channel that is required for possible reattachment (see Section 8). The voltage gradient, E, is given by the lightning current and channel properties according to

$$E = E_{\text{res}} + E_{\text{ind}} = R(I,t) \cdot I(t) + L\frac{\partial I(t)}{\partial t}, \tag{1}$$

where $I(t)$ is the lightning current, R is resistance per unit length of the channel and L is the inductance per unit length.

The shape of the lightning current during the continuing current phase is trivial. However, the shape of the current during the current impulses (return strokes and recoil leaders) must be carefully considered, especially since its time derivative is required in the expression of the inductive part of the voltage gradient of the lightning channel. In the search for an analytical expression for the time-dependence of the current, $I(t)$, appropriate for simulations, the conventional double-exponential function for impulses will not be appropriate here since it gives an infinite derivative of the current at the beginning of the impulse. The IEC function of the lightning current for analysis purposes overcome this problem [22]:

$$I(t) = \frac{I_{\max}}{h}\frac{(t/\tau_1)^{10}}{1+(t/\tau_1)^{10}}\exp\left(-\frac{t}{\tau_2}\right), \tag{2}$$

where $I_{\max}$ is the peak current and h is a correction factor for the peak current, τ_1 and τ_2 are the time constants for the front time and tail time, respectively. The IEC document stipulates the current waveform 10/350 μs ($h = 0.93$, $\tau_1 = 19$ μs, $\tau_2 = 485$ μs) for the first stroke and waveform 0.15/100 μs ($h = 0.993$, $\tau_1 = 0.454$ μs, $\tau_2 = 143$ μs) for subsequent strokes. However, one should bear in mind that the IEC function regards the current at ground for cloud-to-ground lightning flashes. Measured data for the current amplitude and maximum time derivative of the current can be found in the literature [23,9]. For example, as mentioned in the introduction, in-flight measurements give peak currents up to 20 kA and peak time derivatives up to 10^{10} A·s^{-1}. In a practical numerical simulation of the whole flash, the time step required to resolve the

current impulses would imply a long computational time. Instead of simulate the detailed behaviour, one may assume that the impulse take place during only one time step with a given peak current and a given time derivative. Such an approach also eliminates any assumptions about the real shape of the current during return strokes and recoil leaders.

The inductance per unit length of the lightning channel can be approximated by the one of an isolated conductor of radius r_c and of length $h \gg r_c$ as given by [24]

$$L \approx \frac{\mu_0}{2\pi} \ln\left(\frac{h}{r_c}\right) = 0.2 \cdot \ln\left(\frac{h}{r_c}\right) \ \mu\text{H}\cdot\text{m}^{-1} \tag{3}$$

which is plotted in Fig. 7. As can be seen in the figure, the inductance per unit length is only weakly dependent o the channel radius and is roughly constant about $2.0 \pm 0.5\ \mu\text{H}\cdot\text{m}^{-1}$. Thus, a constant value of $2\ \mu\text{H}\cdot\text{m}^{-1}$ is an adequate approximation of the magnitude of the inductance per unit length of the lightning channel.

Typical values for the resistance per unit length of a lightning channel during return stokes are in the range $0.01–0.1\ \Omega\cdot\text{m}^{-1}$ [24]. However, the resistance of the channel has a complex time and current dependence. The resistance will be further discussed in the next section.

Trivially, the resistive current will dominate the build-up of the voltage gradient during the continuing current phase. However, the situation is not that obvious during return strokes and recoil leaders. The contribution by the inductance can be estimated by

$$E_{\text{ind}} = L \cdot \frac{\partial I}{\partial t} \approx 2 \cdot 10^6 \times 10^{11} = 2 \cdot 10^5\ \text{V}\cdot\text{m}^{-1} \tag{4}$$

and the contribution by the resistance

$$E_{\text{res}} = R \cdot I \approx 0.1 \times 20 \cdot 10^3 = 2 \cdot 10^3\ \text{V}\cdot\text{m}^{-1}. \tag{5}$$

Thus, $E_{\text{ind}} \gg E_{\text{res}}$ and the voltage gradient that is inductively built-up clearly dominate, and it is clear that very high values of the internal field are generated allowing longer jumps of the channel. The decay of conductivity of the channel after the transient current phase of the return strokes and the recoil leaders has to be recognised, as well as the development of the resistance of the channel during the zero-current intervals.

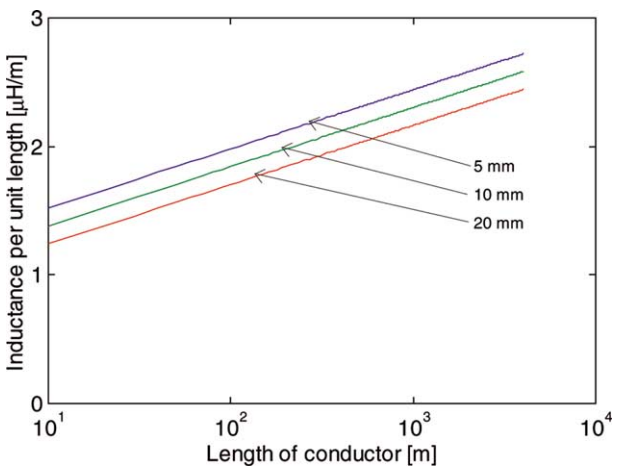

Figure 7. The inductance per unit length of an single conductor according to Eq. (3) for three different values of the conductor radius (5 mm, 10 mm and 20 mm).

Gallimberti and Stangherlin [25] calculated the thermal decay of leader channel when no current flows through it. The initial temperature profile was assumed to have a Gaussian shape. For a temperature maximum of 5000 K and a Gaussian radius of 0.8 mm, the maximum temperature of the channel decays to a value below 1500 K in about 1.2 ms. The limiting value of 1500 K was chosen since below that temperature the electrons stay attached to oxygen molecules. A decay time constant of about 1 ms is consistent with the studies of Lowke et al. [26]. Furthermore, Aleksandrov et al. [27] have studied the channel decay for the situation when the current impulse is followed by a continuing current, where the channel decays to a steady-state situation after a duration of the order of 1 ms.

6. Channel properties

6.1. Initial practical considerations

Maecker [28] describes an arc discharge channel as a region of hot air with strong temperature gradients and that the movement of the channel can be viewed as a heat wave. The position of such an entity could then be defined as the position of its temperature maximum. This description is pertinent also for the channel of the lightning leader channel, of the return stroke and of the recoil leader, since all of them are hot discharges. The motion of the arc channel can be described as a temperature cloud where the motion is divided into two parts, one being the relative velocity of the arc channel with respect to the mass flow and the other the mass motion itself. The motion of the arc channel is then identical to the displacement of its temperature maximum. The velocity of the position of the temperature maximum of the arc channel v_a can thus be divided into two components

$$v_\mathrm{a} = v_\mathrm{am} + v_\mathrm{m}, \tag{6}$$

where v_am is the relative velocity of the position of the maximum temperature with respect to matter and v_m the mass velocity. v_am is determined by the internal energy equation and is zero for situations with axial symmetry of the channel. An example of a channel with broken axial symmetry is a curved channel as illustrated in Fig. 8. A simple formula for the velocity of this 'anti-bending' is [28]

$$v_\mathrm{am} = -5k\frac{\kappa}{n\mathrm{C_p}}, \tag{7}$$

where k is the curvature of the channel (that is, the inverse of the curvature radius), n is the heavy-particle number density and $\mathrm{C_p}$ is the heat capacity at isobaric transformations. Fig. 9 shows the anti-bending velocity as a function of the curvature at two different channel temperatures ($T = 5$ kK and 10 kK, respectively). Considering typical aircraft speeds, Eq. (7) gives that the curvature must be larger than

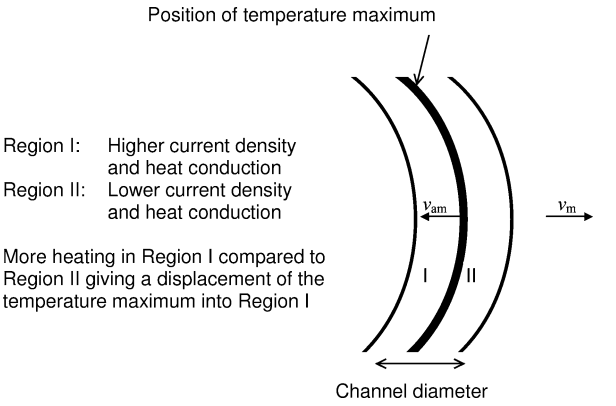

Figure 8. Illustration of the velocity of the mass flow v_m and the relative velocity of the arc channel to the mass flow v_am. The 'anti-bending' of the channel is also explained.

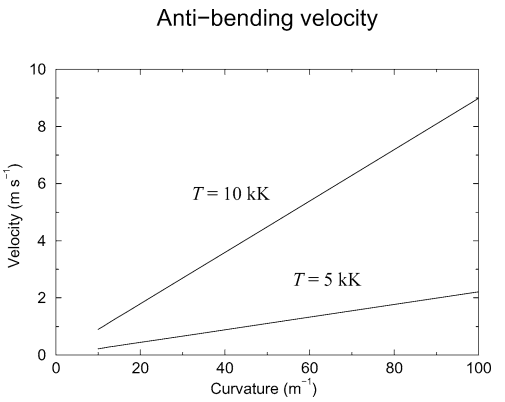

Figure 9. The anti-bending velocity as a function of the channel curvature for two different channel temperatures (5 kK and 10 kK).

100 m^{-1} to give rise to a significant anti-bending velocity. A curvature of 100 m^{-1} is equivalent to a curvature radius of 10 mm, which is close to the radius of the channel. Hence, for the anti-bending to be of importance, there must be a very sharp turn in the arc channel. Consequently, the error introduced by neglecting the anti-bending is small. On the other hand, it is straightforward to include (7) in any swept-stroke simulation.

6.2. Theoretical formulation

The physics of a lightning channel is complex, to say the least. One critical assumption often make in theoretical and numerical treatments is that the discharge plasma column is in local thermodynamic equilibrium (LTE). This is not the case in electrical discharges, but it can often be a valid approximation in lightning and arc channels [29,26,30,31]. However, very close to electrodes (a few millimetres), the deviation from LTE can be significant [32]. The deviation from LTE in electrical discharges is due to the fact that the electrons in the channel has a lower mobility than the positive ions and thus gain more kinetic energy from the electric field. Since the kinetic energy transfer in collisions between light electrons and heavy neutrals is low, no temperature equilibrisation takes place. However, when the ionisation degree approaches about 1%, the coulomb collisions between the electrons and the ions becomes efficient and temperature equilibrisation will take place [33]. This degree of ionisation is normally reached when the temperature of the neutrals becomes so high that thermal ionisation becomes efficient, which occurs around 6000 K in air at atmospheric pressure. The kinetic energy transfer in collisions between ions and neutrals is efficient since these two species have about the same mass. But still, due to the lower mobility of electrons, the electrons will have a slightly higher temperature than the ions and the neutrals. This temperature is, however, in most cases negligible [31].

Once LTE has been established, this equilibrium is sustained even if the electric field falls below the one required forming the LTE [25,31]. Thus, a plasma in LTE can have a lower temperature than the temperature required to form the LTE. The physical reason for this difference in temperature is found in the difference in the mechanisms by which the electrons acquire the energy necessary to ionise the neutrals. In non-LTE plasmas, the electrons receive all energy directly from the field, but in LTE plasmas they also gain energy from collisions with heavy particles.

The implication of the LTE assumption is that there is a unique temperature equal for every kind of particle which makes it possible to treat the arc plasma as a one-phase medium having a well-defined density, velocity and temperature (or energy) at each point. The arc plasma is thus treated as a Newtonian fluid including electromagnetic effects, a frequent found treatment in the literature of arc and lightning modelling [34–39,27]. The balance equations for mass, momentum and total energy can be written as

$$\frac{\partial}{\partial t}(\rho) + \nabla \cdot (\rho \mathbf{v}) = 0, \tag{8}$$

$$\frac{\partial}{\partial t}(\rho \mathbf{v}) + \nabla \cdot (\rho \mathbf{v}\mathbf{v}) = -\nabla p + \nabla \cdot \mathbf{T} + \mathbf{f}_{\mathrm{em}}, \tag{9}$$

$$\frac{\partial}{\partial t}(\rho w) + \nabla \cdot (\rho w v) = -\nabla \cdot Q - S_r + P_J \tag{10}$$

with an equation of state

$$\rho = F(T, p), \tag{11}$$

where ρ is the mass density, $\mathbf{v}$ is the gas velocity, p is the pressure, $\mathbf{T}$ is the momentum diffusion tensor and Q is the thermal diffusion flux. The total energy per unit mass w is related to the temperature T through

$$w = c_{\mathrm{V}} T + \frac{1}{2} v^2, \tag{12}$$

where c_{V} is the heat capacitivity (heat capacity per unit mass).

$S_{\mathrm{r}} = S_{\mathrm{rad}} - S_{\mathrm{abs}}$ are the radiation and absorption of electromagnetic energy, respectively, $P_{\mathrm{J}} = \mathbf{j} \cdot \mathbf{E}$ is the Joule source term where $\mathbf{j}$ is the conduction current density and is given by Ohm's law: $\mathbf{j} = \sigma \mathbf{E}$ where σ is the electrical conductivity. $\mathbf{f}_{\mathrm{em}} = q\mathbf{E} + \mathbf{j} \times \mathbf{B}$ is the total electromagnetic force per unit volume (or the Lorentz force per unit volume), where $\mathbf{B}$ is the magnetic flux density and q is the electric charge density. The magnetic flux density is given by one of the Maxwell's equations:

$$\nabla \times \mathbf{B} = \mu_0 \left(\mathbf{j} + \frac{\partial \mathbf{D}}{\partial t} \right), \tag{13}$$

where μ_0 is the permeability of free space. The second term is the displacement current and it is often neglected in discharge plasma channel modelling. The external lightning current I is related also to the internal electric field via Ohm's law according to

$$I = \int \mathbf{j} \cdot \mathbf{dS} = \int \sigma \mathbf{E} \cdot \mathbf{dS}, \tag{14}$$

where the integration can be taken over the area $\mathbf{S}$ of one of the electrodes. Since the boundary conditions for electromagnetic properties often can easily be stipulated in potentials, the introduction of the scalar, φ, and vector, $\mathbf{A}$, potentials are common:

$$\mathbf{E} = -\nabla \varphi - \frac{\partial \mathbf{A}}{\partial t}, \qquad \mathbf{B} = \nabla \times \mathbf{A}. \tag{15}$$

The energy balance equation ought to contain also the energy density stored in the electromagnetic field w_{em} as given by [40]

$$w_{\mathrm{em}} = \frac{1}{2}(\mathbf{E} \cdot \mathbf{D} + \mathbf{H} \cdot \mathbf{B}) = \frac{1}{2}\left(\varepsilon_0 E^2 + \frac{1}{\mu_0} B^2 \right), \tag{16}$$

where ε_0 and μ_0 are the permittivity and permeability of free space, respectively. This term is often neglected in models of discharge channels. This assumption can be justified, especially in our case where the lightning current is explicitly given and thus the change in the electromagnetic field is implicitly given by the current. Depending on the applications, the different species (atoms, molecules, ions) must be traced. If so, the overall mass conservation Eq. (8) must be completed with mass conservation equations for all involved individual species. If LTE cannot be assumed, the equation system must include energy equations where the participating species have an own temperature or internal energy. Other phenomena that in principle are included in the formulation above, but still might require special attention, are plasma instabilities and

plasma waves [41]. However, probably the most important phenomenon that requires special treatment is turbulence. Small asymmetries in the pressure and the density gradients in the discharge channel is a significant source of vorticity [42]. Attempts to model the turbulence in arc channels are found in the literature [43]. Finally, when a decent description of the discharge channel has been formulated, one must evaluate the effect of the volatile environment that may contain strong wind velocity gradients and heavy turbulence as well as heavy rain.

The exposé above regarding the full formal treatment of the lightning discharge shows that it is impossible to solve the general problem of lightning discharges analytically. Further, even with the enormous development of computers and numerical algorithms, it is today impossible also to solve the general problem numerically. To still take advantage of the powers of numerical simulations, one has to make certain assumptions and simplifications of the theoretical formulation. However, these assumptions and simplifications must be physically justified, not only made to make the simulations easier. Furthermore, the results of all numerical simulations must be confronted with the reality, that is, compared with experimental results. The next section contains an example of a simplification of the full theoretical formulation including a discussion of its assumptions and a comparison with relevant experimental data.

6.3. Simple isobaric model

In this section, a simple model for the lightning channel during the continuing current phase is presented and its applicability is discussed. The continuing current does not vary in time and the thermal energy transport is sufficiently slow to justify that pressure equilibrium is realised everywhere [25]. This means that the pressure is constant in the channel and is equal to the ambient pressure, implying that the momentum balance equation above can be omitted and that the derivatives of the pressure disappear in the energy balance equation. Furthermore, for the current regime of the continuing current, the electromagnetic force can be neglected [44]. One can now write the system as [16,25]

$$\begin{cases} \rho c_p \frac{\partial T}{\partial t} = \kappa \frac{\partial^2 T}{\partial r^2} + \left(\frac{\kappa}{r} + \frac{\partial \kappa}{\partial r} - \rho c_p v_r \right) \frac{\partial T}{\partial r} + \sigma E^2, \\ \rho v_r = -\frac{1}{r} \frac{\partial}{\partial t} \left(\int_0^r r' \rho \, \mathrm{d}r' \right) \end{cases} \tag{17}$$

with the following relationship between the internal electric field E and the lightning current I

$$I = 2\pi E \int_0^R \sigma r \, \mathrm{d}r, \tag{18}$$

where c_p is the heat capacitivity (heat capacity per unit mass) and κ is the thermal conductivity. The initial condition for the temperature was a Gaussian distribution, which is consistent with the radial density profile derived from Schlieren pictures of leader channels [25]. The sensitivity of the results for changes in the initial temperature profile was checked by varying the initial temperature maximum T_0 and the Gaussian radius a. The temperature and radius of a lightning return stroke are about 30 kK and less than 10 mm, respectively [29]. Corresponding values for the laboratory leader channel are 5 kK and 1 mm [45]. The initial properties of the lightning channel before the continuing current phase lies probably somewhere in between these values. Fig. 10 shows four simulations in the case of a constant current of 500 A with four different initial conditions ($T_0 = 20$ kK, $a = 10$ mm; $T_0 = 15$ kK, $a = 10$ mm; $T_0 = 10$ kK, $a = 10$ mm; $T_0 = 15$ kK, $a = 5$ mm) at six different times ($t = 0$, 20, 40, 60, 80 and 100 ms). The figure reveals that at 20 ms and onward, the temperature profiles overlap. Thus, the choice of the initial temperature profile has no significant effect on the later profiles.

The development in time of the internal electric field for two magnitudes of the current is presented in Fig. 11. The internal electric field approaches quite quickly a relatively stable value. Experimental data for

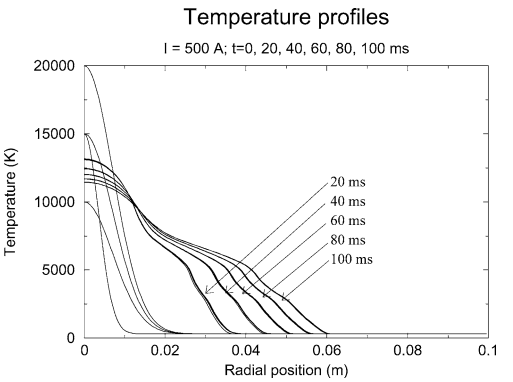

Figure 10. Temperature profiles for four different choices of initial profiles of the temperature ($T_0 = 20$ kK, $a = 10$ mm; $T_0 = 15$ kK, $a = 10$ mm; $T_0 = 10$ kK, $a = 10$ mm; $T_0 = 15$ kK, $a = 5$ mm). The differences in the initial profiles have minor effect on the later profiles.

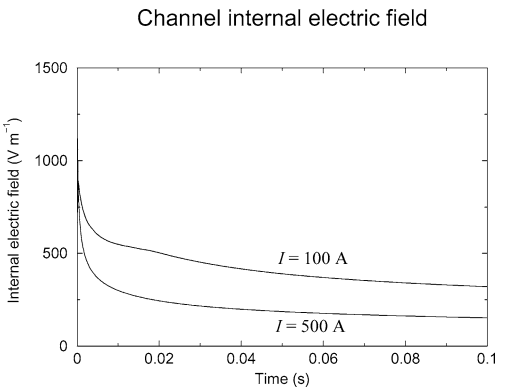

Figure 11. The development in time of the internal electric field for two different arc currents (100 A and 500 A).

the internal field in short (50–500 mm) steady-state free-burning arcs are given by von Engel [46]. In the current range of 100 A–1 kA, the internal electric field of an arc channel is 200–150 V·m^{-1}, thus being only slightly dependent on the magnitude of the current. The simulations gives a larger dependency, but the magnitude of the internal electric field is in good agreement with the measurements. Thus, for these steady-state arcs, the assumption of a cylindrical plasma channel is validated.

During the swept stroke, the arc channel might be elongated: the length, and thereby the volume, of the channel increases. This elongation cannot be directly included into the arc column model presented in above since the elongation is a process in the axial direction. However, the channel elongation can be introduced as an artificial energy loss term, Q_{elo}, in the energy-balance equation. Q_{elo} is taken equal to the energy that is required to heat all the extra volume of air in the channel to the channel temperature. In our case of a cylindrical and isobaric channel that is elongated with velocity v_{elo}, Q_{elo} is given by [16]

$$Q_{\mathrm{elo}} = 2\pi v_{\mathrm{elo}} r \,\mathrm{d}r \int_{T_{\mathrm{amb}}}^{T} \rho c_{\mathrm{p}} \,\mathrm{d}T', \tag{19}$$

where $T = T(r)$ is the channel temperature and T_{amb} is the temperature from which the air in the extra volume must be heated. The influence of the elongation velocity for a continuing current of 100 A is shown in Fig. 12. The figure shows the development in time of the resistance per unit length of the channel. The initial conditions for the channel temperature profiles are a Gaussian radius of 10 mm and a maximum temperature of 14 kK. These and further estimates of the influence of the channel elongation give that the channel elongation velocity must be significantly above 1000 m·s^{-1} to give any recognisable contribution. Thus, for the arc channel during the lightning swept stroke along aircraft, the effect of channel elongation is negligible.

6.4. Long arc experimental data

Tanaka et al. [47] have studied long arcs (1.2–3.2 m) subjected to continuing currents (100–2000 A) with a duration of up to 100 ms. They conclude "*free arcs, which have no restrictions such as a stabilising wall or forced external flow, show complex motion due to the effects of electromagnetic force and natural convection flow*". The complex tortuous path of the channel has been estimated to be 1.5–2.0 times longer than the axial distance between the electrodes. With this tortuous path, the internal electric field strength of

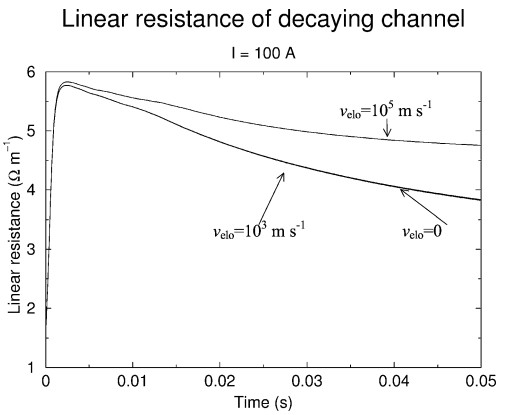

Figure 12. The development in time of the resistance per unit length (linear resistance) of the arc channel at different magnitude of the elongation velocity v_{elo} for a current of 100 A. Note that the curves for $v_{\mathrm{elo}} = 0$ and $v_{\mathrm{elo}} = 1$ km·s^{-1} overlap. The initial conditions for the channel temperature profile are a Gaussian radius of 10 mm and a maximum temperature of 14 kK.

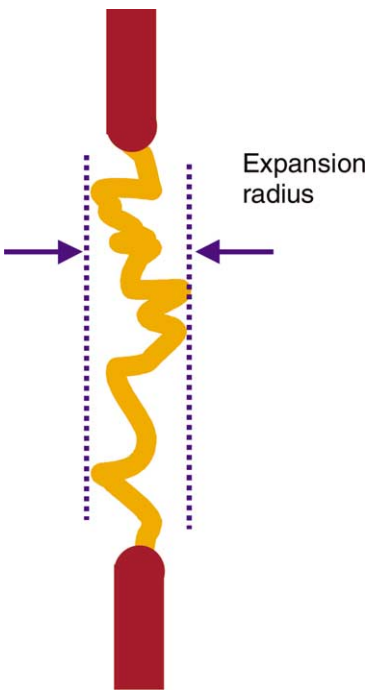

Figure 13. An arc discharge between two rod electrodes where the expansion radius is illustrated.

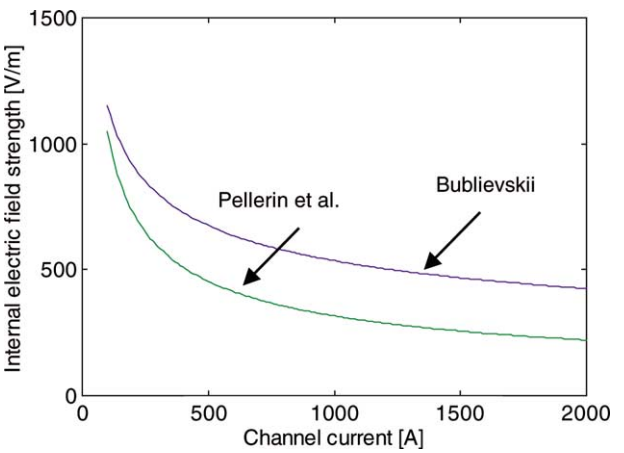

Figure 14. The internal electric field strength as a function of the lightning current according to the formulas given by Bublievskii and Pellerin et al., respectively, with a speed of the perpendicular aerodynamic flow of 5 m·s^{-1}.

the channel was estimated to be 450–700 V·m^{-1}. The tortuous motion of the channel reaches a maximum distance from the central axis of the electrode gap; a distance called *the expansion radius*, as illustrated in Fig. 13. This expansion radius was measured to be 0.1–0.2 m. The channel shows a random motion within the expansion radius with a speed of up to 10 m·s^{-1} [48]. Two theoretical treatments give the internal electric field strength as a function of both the current and the airflow velocity. Bublievskii studied the thermal losses of an arc channel that was balanced by aerodynamic and magnetic fields [49]. Pellerin et al. studied the behaviour of a magnetically driven arc, so-called 'glidarc' [50]. They reached to the following expressions for the internal electric field

$$E_{\mathrm{Bub}} = 1.83 \times 10^3 \left(\frac{v^2}{I}\right)^{1/3}, \tag{20}$$

$$E_{\mathrm{Pel}} = 5.3 \times 10^3 \frac{v^{0.48}}{I^{0.52}}, \tag{21}$$

where I is the lightning current and v is the velocity of the airflow perpendicular to the arc channel. These functions are plotted in Fig. 14 and give consistent results when comparing to the experimental data provided by Tanaka et al.

7. Attachment point phenomena

The attachment point serves as the origin of two different threats to the aircraft. Firstly, they determine the current distribution in the airframe and thereby the electromagnetic compatibility threat. Secondly, the points are heated by the lightning current and thereby are the locations of damage and destruction of the materials. The attachment point phenomena, or electrode processes, constitute one of the most complex problems within the field of discharge physics. Both the anode (exit point) processes and the cathode (entry point) processes are complex [31], but most attention has been paid to the cathode. See, for instance, the reviews by Jüttner [51] and Guile [52] and the references therein. The cathode processes are more of interest when looking at the general behaviour of an electrical discharge since the cathode must eject the charger carriers (electrons) where the anode 'only' is required to collect them. However, for the application of aircraft hazards, they are of equal interest when consider the current distribution in the airframe and probably also of equal interest when consider the thermal damage of the materials. However, even for the aircraft hazard application, most attention has been paid to the effects at the cathode [53,54].

Laboratory experiments pertinent to aircraft applications [55,56] show that the discharge channel either sweeps continuously along a bare metal surface or that it dwells shortly (a few milliseconds) at each attachment point. Apparently, even for these similar studies the results disagree. Furthermore, one must consider all different possible situations: Bare metal surfaces, surfaces with preferred attachment points such as edges and rivets, painted metal surfaces, composite surfaces and metalised composite surfaces. The continuous sweeping of a lightning channel along an aircraft can be understood in the following way. A qualitative electric field calculation of the situation is presented in Fig. 15. The distribution of the aerodynamic flow, in particular the structure of the boundary layer, will deform the channel in the vicinity of the surface. A consequence of this deformation is that the electric field lines and the current density at the attachment point will be concentrated downstream the channel, resulting in an increased heating of this part of the channel. Thus, the channel will be displaced in the direction of the aerodynamic flow. The thickness of the boundary layer together with the channel radius determines the region of continuous sweeping. The channel can be assumed to follow the background flow above the boundary layer if the channel radius of

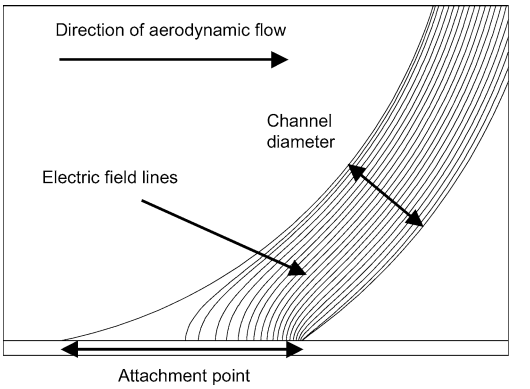

Figure 15. Electric field calculation for a channel with significantly higher conductivity than the surroundings. The figure shows the electric field lines, which is clearly concentrated downstream the channel within the attachment point.

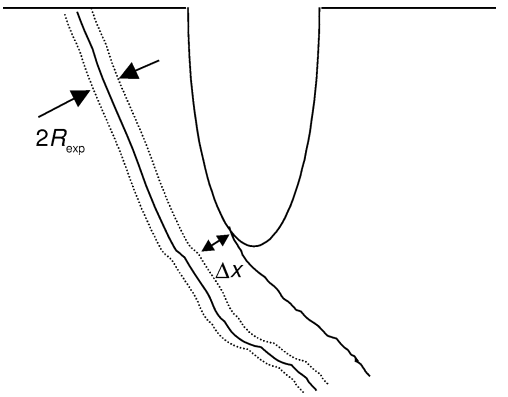

Figure 16. Illustration of how the lightning channel can reattach to the wing. The solid line represents the central axis of the channel and the dotted line marks the region determined by the expansion radius R_{exp}. Δx is the distance between this region and the aircraft.

the channel is equal to, or greater than, the thickness of the boundary layer. If this assumption is valid, the non-viscous approximation of the aerodynamic flow is pertinent. For our application, it is the expansion radius that mainly determines the region of continuous sweeping, not the channel radius. For a discussion about the expansion radius, see Section 6.4 and Fig. 13.

8. Reattachment process

Reattachment occurs when the potential drop along the channel together with the channel displacement and deformation due to the aerodynamic flow create a situation where there is a favourable condition for an electrical breakdown between a segment of the channel and the surface, as illustrated in Fig. 3(c). After the reattachment, the channel has a new attachment point and part of the channel is short-circuited. The distance between two consecutive attachment points is called the 'skip distance'. Since the geometry of an aircraft is complex, reattachment of the lightning channel may occur to parts far from the attachment point, which lead to a significant jump of the point. This may happen if any other part of the aircraft comes within the expansion radius of the channel (cf. Section 6.4 and Fig. 13). In such a case, the channel gets in contact with that part and a new attachment point is created. The situation is illustrated in Fig. 16, with $\Delta x = 0$, where Δx is the distance between the aircraft and the region determined by the expansion radius of the channel.

Reattachment with $\Delta x > 0$ will occur if there is a favourable condition for dielectric breakdown of the air gap between the lightning channel and the surface of the aircraft. A simplified expression for this condition is:

$$V_{\text{p}} > E_{\text{B}} \cdot \Delta x, \tag{22}$$

where V_{p} is the potential at point 'p' along the channel, and E_{B} is the critical field for dielectric breakdown of the air. However, this condition is unlikely to be fulfilled during the continuing current phase because the voltage gradient along the channel is too small. On the other hand, during return strokes and recoil leaders, the voltage drop along the channel is significantly increased according to Eq. (1) and reattachment may be likely.

The condition (22) has to be modified if the surface is covered by a dielectric layer, for instance, being painted. The condition becomes

$$V_{\text{p}} > E_{\text{B}} \cdot \Delta x + E_{\text{Bdiel}} \cdot e_{\text{diel}}, \tag{23}$$

where E_{Bdiel} is the critical field for dielectric breakdown of the dielectric material and e_{diel} is the thickness of the dielectric layer. If this condition is fulfilled, the dielectric layer will be punctured, and a new attachment point will be formed.

In the breakdown criteria introduced above, it is assumed that the electric field is uniform between the channel and the aircraft, and that the air and the painted layers have well-defined critical electric field strengths for dielectric breakdown. The technique for calculating the electric field distribution during a lightning strike to an aircraft is highly developed [57]. Further, detailed air discharge models also exist [58,59]. A combination of advanced electric field calculations with a detailed air discharge model would solve the problem of reattachment to a high degree of accuracy but to the cost of enormous computation time. However, the reattachment criteria as stated above give sufficient accuracy for the intended application.

9. An algorithm for swept stroke simulations

The roadmap of swept stoke simulations, as illustrated in Fig. 4, has been implemented into a swept stoke code at ONERA. The code has a generic structure where all influencing factors are included with individual sub-models. All these sub-models can be independently refined to a sufficient degree. The algorithm of the ONERA code is as follows (Fig. 17): the aircraft geometry and the aerodynamic flow profile are required as input data as well as the lightning current. For a given direction of the background electrostatic field, the initial attachment points are given via the inception model. With this information, the properties and locations of the initial lightning channels are calculated. When all initiations are done, the main loop is entered. In this loop, the channel displacement is determined. If having continuous sweeping, the attachment points are displaced along the surface. The breakdown conditions are then checked along the entire channel

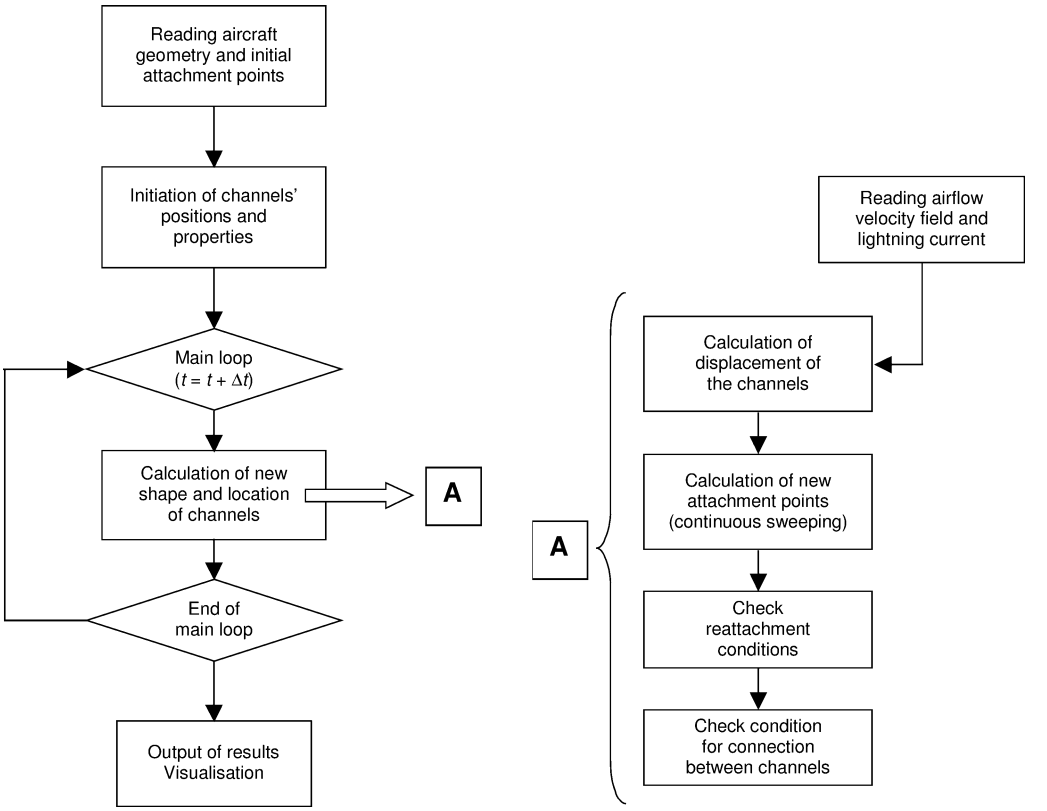

Figure 17. The general algorithm for the swept stroke calculation as implemented in the ONERA code.

to determine if reattachment occurs. Finally, it is checked if there will be a connection between the two channels.

10. Examples of swept stoke simulations

10.1. Rocket sled experiment

The most realistic swept-stroke experiment found in the literature is presented by Dobbing and Hansson [60] where they used a moving test vehicle and a stationary arc. The test vehicle was a wing dummy mounted on a rocket sled running on a railway, which intercepted the stationary arc. The arc was initiated by an exploding wire and the current was delivered from an inductive storage arc generating system. The arc current was in the range of 300–600 A and a typical rocket sled speed was 52 $\mathrm{m{\cdot}s^{-1}}$.

One test series was with an aluminium wing dummy that was painted. Since the surface was painted, no continuous sweeping was present and a series of reattachments was observed according to the scenario shown in Fig. 3(c). With the skip distance (the distance between the attachment points) and the measured voltage along the arc, they estimated the mean voltage gradient of the arc to be

$$E_{\mathrm{arc}} = 1.34 \pm 0.44\ \mathrm{kV{\cdot}m^{-1}}. \tag{24}$$

When the wing dummy intercepted the arc channel, they observed that the channel was in contact with the surface along the whole part of the channel that was deformed by the boundary layer, which implies that the thickness of the boundary layer was smaller than the channel radius (or within the region of the expansion radius of the channel). Furthermore, they observed no influence of polarity (entry and exit points of the current behaved similar).

The simulation of the rocket-sled experiment was performed with a 2D version of the swept stroke code. For this case of a planar surface, an aerodynamic flow according to the Blasius profile was used [61]. Fig. 18 illustrates the results of such a swept-stroke simulation with an aerodynamic flow velocity of 52 $\mathrm{m{\cdot}s^{-1}}$ and an arc current of 600 A [17]. In the simulation, the boundary layer thickness was set to 5 mm but was considered to be smaller than the channel radius. In the figure, the position of the temperature maximum is shown and the successive reattachments are clearly seen. The calculation gives a mean voltage gradient of 1.8 $\mathrm{kV{\cdot}m^{-1}}$ of the short-circuited part of the arc channel at reattachment (dwell time 7.4 ms, skip distance 0.39 m). This value of the voltage gradient is on the upper boundary of the measured one according to (24). Larsson et al. [17] give more details about the 2D simulations.

10.2. Swept stokes along aircraft

In this section, examples of swept stroke calculations on real aircraft geometries are presented. An example of a simulation of a nose-wing strike to a B737 aircraft is shown in Fig. 19. In this example, the

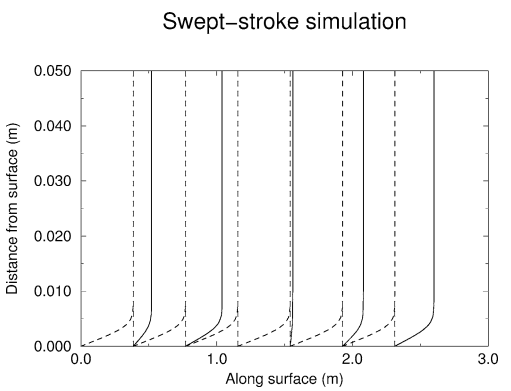

Figure 18. A numerical simulation of a swept stroke along a painted surface with an aerodynamic flow velocity of 52 $\mathrm{m{\cdot}s^{-1}}$ and an arc current of 600 A where the channel radius is greater than the thickness of the boundary layer. The solid lines are snapshots of the position of the arc channel at regular time intervals (time interval between snapshots: 10 ms). The dashed lines show the arc channel just before and just after a reattachment. Note the different scales on the axes.

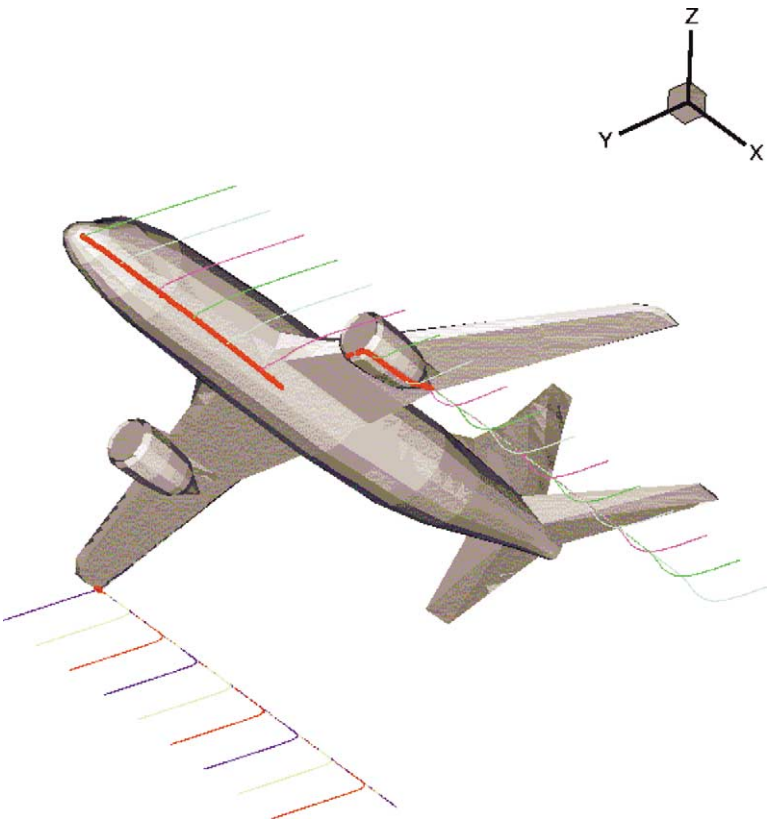

Figure 19. Swept stoke simulation of a nose-wing strike to a B737 aircraft where the continuous sweeping of the channel is illustrated as well as the reattachment to other parts of the aircraft, in this case the left engine. The dwelling of the attachment point at the same location at the right wing is also clearly visible.

first attachment point at the nose is continuously swept along the underside of the fuselage until it reaches the region of the wing and engine, where the channel reattach to the engine and continue its continuous sweeping along it. The attachment point on the wing dwells at the same location since it cannot be swept any further. Another example is shown in Fig. 20 where a nose-tail strike has been simulated for a C-160 aircraft. The figure shows only the displacement of the nose part of the channel. Here, part of the fuselage is covered with a dielectric layer that hinders the continuous sweeping. The dwelling of the channel at the border of the dielectric layer and the elongation of the channel are clearly visible. In this example, the dielectric layer is punctured and a new attachment point is formed. When the channel has passed the dielectric layer, the channel continues to sweep along the fuselage and later along the wing.

11. Conclusions and future challenges

The mechanisms of the lightning strike to aircraft are described in this article and the important issues for the lightning swept stroke are outlined and an implementation is presented. The real future challenge is the validation of the simulation tool. Dedicated experimental studies in the laboratory must be designed and conducted in order to achieve appropriate data to compare with. And finally, the simulations must be confronted with real incidents of lightning strikes to aircraft. With an appropriate database of experimental results, the results of the simulations can be estimated and possible weaknesses of the model can be identified.

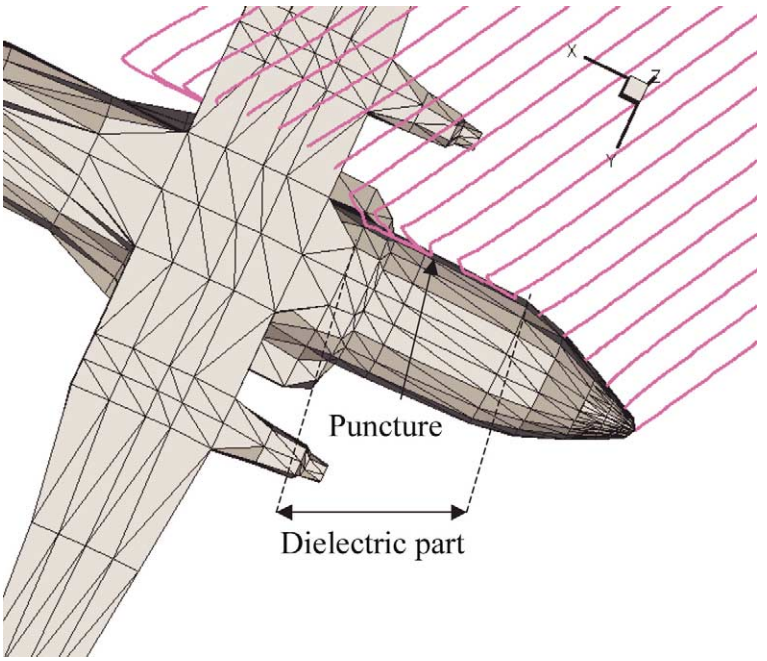

Figure 20. Detail of the sweeping simulation in case of a nose-wing strike to a C-160 aircraft. The part of the fuselage that is covered with a dielectric layer is marked in the figure as well as the location of the puncture at the point of reattachment.

Acknowledgements. This work was initiated during a one-year postdoctoral visit by the author at the Atmospheric Environment Research Unit at ONERA, France, and its manager Dr Pierre Laroche is sincerely thanked for providing a stimulating scientific environment and for providing the means for that visit. The contribution by my colleagues at ONERA, Anne Bondiou-Clergerie, Philippe Lalande and Alain Delannoy, is greatly acknowledged.

References

[1] B. Fisher, R. Taeuber, K. Crouch, Implications of a recent lightning strike to a NASA jet trainer, AIAA Paper 88-0394, AIAA 26th Aerospace Sciences Meeting, Reno, USA, 1988.
[2] Ch. Jones, D. Rowse, G. Odam, Probabilities of catastrophe in lightning hazard assessments, Paper No 2001-01-2877, Int. Conf. on Lightning and Static Electricity, Seattle, USA, 2001.
[3] M. Severin, B. Wahlgren, The European project EM-Haz: A consolidated approach to the electromagnetic threat, Paper No 2001-01-2878, Int. Conf. on Lightning and Static Electricity, Seattle, USA, 2001.
[4] V. Mazur, Lightning threat to aircraft: do we know all we need to know?, J. Aircraft 30 (1993) 156–159.
[5] B. Fisher, P. Brown, A. Plumer, A. Wunschel, Final results of the NASA storm hazards program, Int. Aerospace and Ground Conf. on Lightning and Static Electricity, Oklahoma, USA, NOAA Special Report, 1988.
[6] J.S. Reazer, A.V. Serrano, L.W. Walko, H.D. Burket, Analysis of correlated electromagnetic field and current pulses during airborne lightning attachments, Electromagnetics 7 (1987) 509–539.
[7] J.-P. Moreau, J.-C. Alliot, V. Mazur, Aircraft lighting initiation and interception from in situ electric measurements and fast video observations, J. Geophys. Res. 97 (1992) 903–912.
[8] F. Uhlig, C. Jones, M. Vile, B. Tagliana, Setup and statistical analysis of an database on in-flight lightning strike incidents, Int. Conf. on Lightning and Static Electricity, Toulouse, France, 1999.
[9] P. Lalande, A. Bondiou-Clergerie, P. Laroche, Analysis of available in-flight measurements of lightning strikes to aircraft, Int. Conf. on Lightning and Static Electricity, Toulouse, France, 1999.
[10] D.W. Clifford, H.W. Kasemir, Triggered lightning, IEEE Trans. Electromagn. Compatibility 24 (1982) 112–122.
[11] V. Mazur, B. Fisher, J. Gerlach, Lightning strikes to an airplane in a thunderstorm, J. Aircraft 21 (1984) 607–611.

[12] A. Castellani, A. Bondiou-Clergerie, P. Lalande, A. Bonamy, I. Gallimberti, Laboratory study of the bi-leader process from an electrically floating conductor – Part 1: General results, IEE Proc. Sci. Meas. Technol. 145 (1998) 185–192.
[13] A. Castellani, A. Bondiou-Clergerie, P. Lalande, A. Bonamy, I. Gallimberti, Laboratory study of the bi-leader process from an electrically floating conductor – Part 2: Bi-leader properties, IEE Proc. Sci. Meas. Technol. 145 (1998) 193–199.
[14] V. Mazur, Physical processes during development of lightning flashes, C. R. Physique 3 (2002) 1393–1409.
[15] H. Zaglauer, W. Wulbrand, A. Douay, F. Uhlig, C. Jones, K. Clibbon, A. Ulmann, P. Lalande, A. Bondiou-Clergerie, P. Laroche, Definition of lightning strike zones on aircraft and helicopters – results of the FULMEN program, Int. Conf. on Lightning and Static Electricity, Toulouse, France, 1999.
[16] A. Larsson, P. Lalande, A. Bondiou-Clergerie, A. Delannoy, The lightning swept stroke along an aircraft in flight. Part I: thermodynamic and electric properties of lightning arc channels, J. Phys. D 33 (2000) 1866–1875.
[17] A. Larsson, P. Lalande, A. Bondiou-Clergerie, The lightning swept stroke along an aircraft in flight. Part II: numerical simulations of the complete process, J. Phys. D 33 (2000) 1876–1883.
[18] A. Larsson, A. Bondiou-Clergerie, P. Lalande, A. Delannoy, S. Dupraz, New methodology for determining the extension of lightning swept stroke zones on airborne vehicles, Paper No 2001-01-2876, Int. Conf. on Lightning and Static Electricity, Seattle, USA, 2001.
[19] P. Lalande, A. Bondiou-Clergerie, P. Laroche, Computation of the initial discharge initiation zones on aircraft or helicopter, Int. Conf. on Lightning and Static Electricity, Toulouse, France, 1999.
[20] I. Coton, B. McNiff, T. Soerensen, W. Zischank, P. Christiansen, M. Hoppe-Klipper, S. Ramakers, P. Pettersson, E. Muljadi, Lightning protection for wind turbines, Paper No 9.13, 25th Int. Conf. on Lightning Protection, Rhodes, Greece, 2000.
[21] D.J. Tritton, Physical Fluid Dynamics, 2nd edition, Clarendon Press, Oxford, 1988.
[22] IEC 61312-1, Protection against lightning electromagnetic impulse – Part 1: General principles, 1995.
[23] R. Thottappillil, Electromagnetic pulse environment of cloud-to-ground lightning for EMC studies, IEEE Trans. Electromagn. Compatibility 44 (2002) 203–213.
[24] E. Bazelyan, Yu. Raizer, Lightning Physics and Lightning Protection, Institute of Physics, Bristol, 2000.
[25] I. Gallimberti, S. Stangherlin, Thermodynamic decay of the leader channel after the discharge arrest, IEE Proc. A 133 (1986) 431–437.
[26] J.J. Lowke, R.E. Voshall, H.C. Ludwig, Decay of electrical conductance and temperature of arc plasmas, J. Appl. Phys. 44 (1973) 3513–3523.
[27] N.L. Aleksandrov, E.M. Bazelyan, M.N. Shneider, Effect of continuous current during pauses between successive strokes on the decay of the lightning channel, Plasma Phys. Rep. 26 (2000) 952–960.
[28] H. Maecker, Principles of arc motion and displacement, Proc. IEEE 59 (1971) 439–449.
[29] M.A. Uman, R.E. Voshall, Time interval between lightning strokes and the initiation of dart leaders, J. Geophys. Res. 73 (1968) 497–506.
[30] C. Delalondre, O. Simonin, Modelling of high intensity arcs including non-equilibrium description of the cathode sheath, J. Phys. Coll. C5 51 (1990) 199–206.
[31] Yu. Raizer, Gas Discharge Physics, Springer-Verlag, Berlin, 1999.
[32] J. Haidar, Non equilibrium modelling of tranferred arcs, J. Phys. D 32 (1999) 263–272.
[33] H. Tholl, Thermalisierung und zeitliche Entwicklung der Elektonendichte und Temperatur von Funkenkanälen in Wasserstoff, Z. Naturforsch 25a (1970) 420–429.
[34] A. Kaddani, S. Zahrai, C. Delalondre, O. Simonin, Three-dimensional modelling of unsteady high-pressure arcs in argon, J. Phys. D 28 (1995) 2294–2305.
[35] P. Freton, J.J. Gonzalez, A. Gleizes, Comparison between a two- and a three-dimensional arc plasma configuration, J. Phys. D 33 (2000) 2442–2452.
[36] M. Kelkar, J. Heberlein, Physics of an arc in cross flow, J. Phys. D 33 (2000) 2172–2182.
[37] M. Plooster, Shock waves from line sources. Numerical solutions and experimental measurements, Phys. Fluids 13 (1970) 2665–2675.
[38] M. Plooster, Numerical simulation of spark discharges in air, Phys. Fluids 14 (1971) 2111–2123.
[39] M. Plooster, Numerical model of the return stroke of the lightning discharge, Phys. Fluids 14 (1971) 2124–2133.
[40] J.D. Jackson, Classical Electrodynamics, 2nd edition, Wiley, New York, 1975.
[41] G. Schmidt, Physics of High Temperature Plasma, 2nd edition, Academic Press, New York, 1979.
[42] J.M. Picone, J.P. Boris, J.R. Greig, M. Raleigh, R.F. Fernsler, Convective cooling of lightning channels, J. Atmospheric Sci. 38 (1981) 2056–2062.
[43] J.C. Vérité, T. Boucher, A. Comte, C. Delalondre, P. Robin-Jouan, E. Serres, V. Texier, M. Barrault, P. Chevrier, C. Fievet, Arc modelling in SF_6 circuit breakers, IEE Proc. Sci. Meas. Technol. 142 (1995) 189–196.

[44] G.R. Jones, High current arcs at high pressures, XVI Int. Conf. on Phenomena in Ionized Gases, Düsseldorf, Germany, 1983.
[45] I. Gallimberti, The mechanism of the long spark formation, J. Phys. Coll. C7 40 (1979) 193–250.
[46] A. von Engel, Ionized Gases, Clarendon Press, Oxford, 1955.
[47] S. Tanaka, K. Sunabe, Y. Goda, Three dimensional behaviour analysis of DC free arc column by image processing technique, Paper No A41, XIII Int. Conf. on Gas Discharges and their Applications Glasgow, UK, 2000.
[48] K. Sunabe, T. Inaba, Electric and moving characteristics of DC kiloampere high-current arcs in atmospheric air, Elec. Engrg. Japan 110 (1) (1990) 9–20.
[49] A.F. Bublievskii, An approximative model of an electric arc in transverse mutually perpendicular aerodynamic and magnetic fields, J. Engrg. Phys. 35 (1978) 1424–1429.
[50] S. Pellerin, F. Richard, J. Chapelle, J.-M. Cormier, K. Musiol, Heat string model of bi-dimensional DC glidarc, J. Phys. D 33 (2000) 2407–2419.
[51] B. Jüttner, Cathode spots of electric arcs, J. Phys. D 34 (2001) R103–R123.
[52] A.E. Guile, Electric arcs: their electrode processes and engineering applications, IEE Proc. 121 (7) (1984) 450–480, Part A.
[53] R. Brocke, F. Noack, F. Reichert, J. Schoenau, W. Zischank, The numerical simulation on the effects of lightning current arcs at the attachment point, Paper No 2001-01-2873, Int. Conf. on Lightning and Static Electricity, Seattle, USA, 2001.
[54] Ph. Testé, T. Leblanc, F. Uhlig, J.-P. Chabrerie, 3D modelling of the heating of a metal sheet by a moving arc: application to aircraft lightning protection, Eur. Phys. J. 11 (2000) 197–204.
[55] L.L. Oh, S.D. Schneider, Lightning strike performance of thin metal skin, Conf. on Lightning and Static Electricity, Culham, UK, 1975.
[56] A. Bizyaev, M. Bourmistrov, L. Levitova, V. Noskov, E. Prokhorov, E. Sobolevskaya, K. Sokolov, T. Tarasova, A. Douay, B. Tagliana, F. Uhlig, Investigation of the sweeping of lightning in wind blown arc experiments, Int. Conf. on Lightning and Static Electricity, Toulouse, France, 1999.
[57] A. Castellani, Calcul du champ électrique par la méthode des charges equivalentes pour la simulation d'une déchage bi-leader, Thèse de doctorat, Université d'Orsay, Paris, France, 1995.
[58] A. Bondiou, I. Gallimberti, Theoretical modelling of the development of the positive spark in long gaps, J. Phys. D 27 (1994) 1252–1266.
[59] E.M. Bazelyan, Yu.P. Raizer, Spark Discharge, CRC Press, Boca Raton, 1998.
[60] J.A. Dobbing, A.W. Hanson, A swept stroke experiment with a rocket sled, Int. Symp. on Electromagnetic Compatibility, Atlanta, USA, 1978.
[61] H. Schlichting, Boundary-Layer Theory, 6nd edition, McGraw-Hill, New York, 1968.